25. Amorphous Semiconductors: Structure, Optical, and Electrical Properties

This chapter is devoted to a survey of the structural, optical and electrical properties of amorphous semiconductors on the basis of their fundamental understanding. These properties are important for various types of applications using amorphous semiconductors.

First, we review general aspects of the electronic states and defects in amorphous semiconductors, i.e., a-Si:H and related materials, and chalcogenide glasses, and their structural, optical and electrical properties.

Further, we survey the two types of phenomena associated with amorphous structure, i.e., light-induced phenomena, and quantum phenomena associated with nanosized amorphous structure. The former are important from the viewpoint of amorphous-silicon solar cells. The latter phenomena promise novel applications of amorphous semiconductors from the viewpoint of nanotechnology.

Amorphous semiconductors are promising electronic materials for a wide range of applications such as solar cells, thin-film transistors, light sensors, optical memory devices, vidicons, electrophotographic applications, X-ray image sensors, europium-doped optical-fibre amplifications etc, particularly, hydrogenated amorphous silicon (a-Si:H) for solar cells, thin-film transistors, X-ray image sensors, and chalcogenide glasses for optical memory devices including digital video/versatile disk (DVD). In this chapter, we emphasize the basic concepts and general aspects of the electronic properties of amorphous semiconductors such as their electrical and optical properties as well as their structural properties [25.1–3]. Furthermore, some basic and important results of these properties are described to understand these applications and to consider their further development. Light-induced phenomena in amorphous semiconductors, which have been considered to be associated with amorphous structure, are also described.

Nanosized amorphous structures exhibit quantum effects associated with two-dimensional (quantum well), one-dimensional (quantum wire) and zero-dimensional (quantum dot) structures, so they have received significant attention on both the fundamental and application sides. These topics are briefly described.

25.1 Electronic States

Long-range disorder in amorphous network breaks down the periodic arrangement of constituent atoms, as shown in Fig. 25.1. In the figure, the structures of amorphous and crystalline silicon are shown. The periodic arrangement of atoms makes it easy to treat the electronic states mathematically, i.e., the so-called Bloch the-

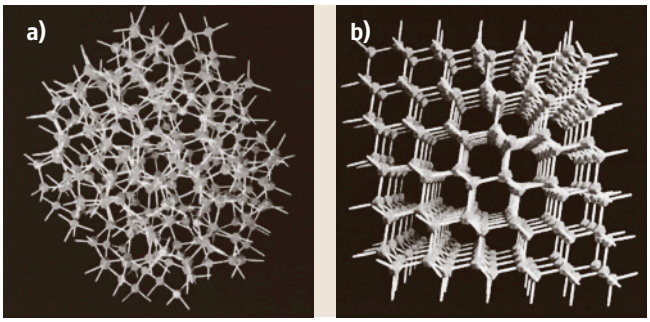

Fig. 25.1a,b Structural models of **(a)** amorphous silicon and **(b)** crystalline silicon

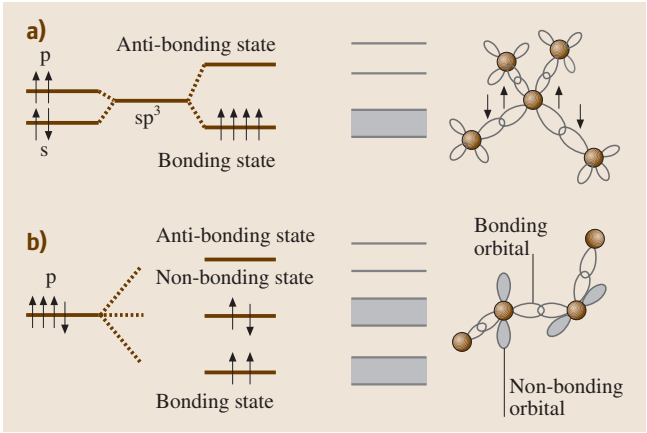

Fig. 25.2a,b Schematic diagram of the energy levels of atomic orbitals, hybridized orbitals and bands for **(a)** tetrahedrally bonded semiconductors, e.g., a-Si and for **(b)** selenium

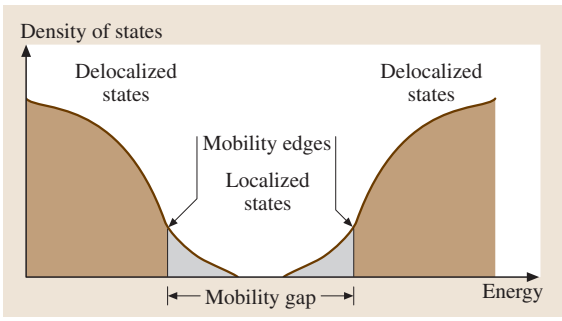

Fig. 25.3 Schematic diagram of the density of states of the conduction band (delocalized states) and the valence band (delocalized states) shown by the *brown-colored*. The mobility edge and mobility gap are shown

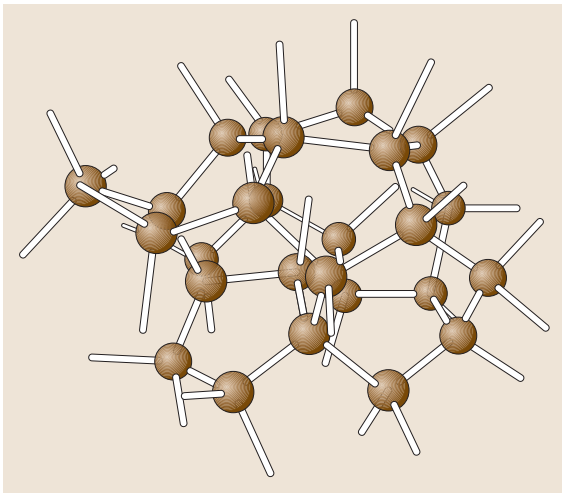

Fig. 25.4 Schematic illustration of a dangling bond in tetrahedrally bonded amorphous semiconductors

ory can be applied to crystalline solids. On the other hand, it becomes difficult to treat the electronic states in amorphous solids mathematically. However, electronic states in amorphous semiconductors are simply described in terms of tight-binding approximations and Hartree–Fock calculations. Using these approaches, spatial fluctuations of bond length, bond angle and dihedral angle lead to broadening of the edges of the conduction and valence bands, constructing the band tail. This is due to spatial fluctuations of bond energy between constituent atoms in tetrahedrally coordinated semiconductors such as Si and Ge, in which the bonding state and the antibonding state constitute the valence band and the conduction band, respectively, as shown in Fig. 25.2a. In chalcogenide glasses, the conduction band arises from the antibonding state, while the valence band arises from the nonbonding state, as shown in Fig. 25.2b. The broadening of those bonds also occurs as a result of potential fluctuations associated with the amorphous network of constituent atoms. The static charge fluctuation associated with bond-length and bond-angle variations in the amorphous network has been discussed theoretically [25.4] and experimentally [25.5, 6] in amorphous silicon.

In the band tails, the electronic states have a localized character and their nature changes from localized to delocalized at a critical boundary called the mobility edge, as shown in Fig. 25.3. The energy separation between the two mobility edges of the conduction and valence bands is called the mobility gap. The nature of the conduction and valence bands has been elucidated by means of photoemission spectroscopy [25.7]. The structure of actual samples of amorphous semiconduc-

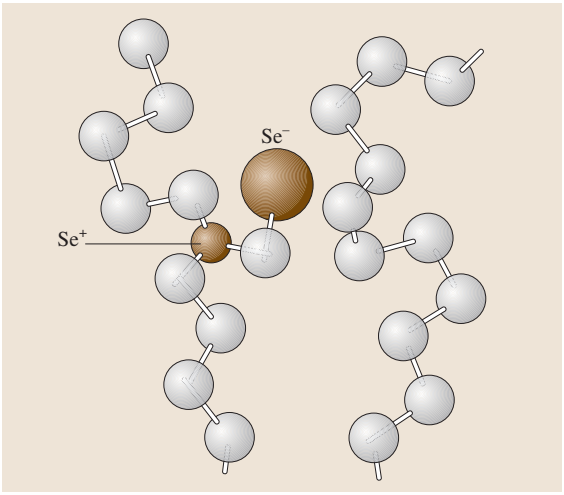

Fig. 25.5 Schematic illustration of two selenium chains with positively charged threefold-coordinated selenium and negatively charged onefold-coordinated selenium

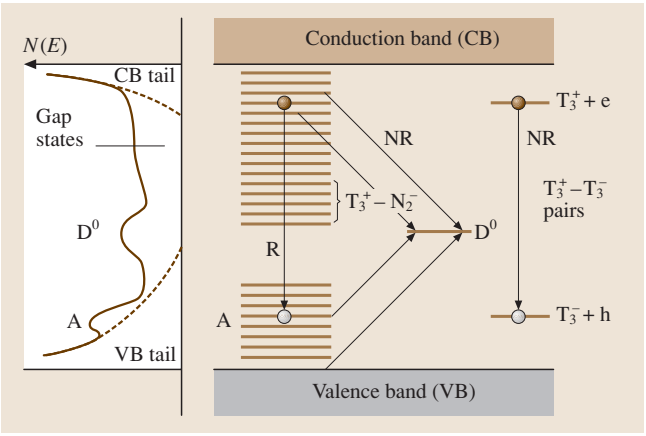

Fig. 25.6 Schematic diagram of the tail and gap states and the recombination processes in a-Si:H. R and NR designate radiative and nonradiative recombination, respectively. A diagram of the density of states spectrum is illustrated on the *left-hand side*. For the definition of other symbols, see the text. (After [25.9])

tors deviates from the ideal random network, namely, coordination of constituent atoms deviates from the normal coordination following the $8-N$ rule [25.1], where N designates the number of valence electrons. For instance, the normal coordinations of Si and Se are four and two, respectively. However, in actual samples Si atoms with a threefold coordination are present in a-Si (Fig. 25.4), and Se atoms with onefold and threefold coordinations are present in a-Se (Fig. 25.5). These atoms are generally called structural defects (gap states) whose electronic energy levels are located within the band-gap region. In the case of chalcogenide glasses, onefold- and threefold-coordinated Se atoms are called valence-alternation pairs (VAP) [25.8]. The detailed properties of structural defects have been elucidated by means of optical spectroscopies such as photoinduced absorption (PA), photothermal deflection spectroscopy (PDS) and the constant-photocurrent method (CPM), capacitance measurements such as deep-level transient spectroscopy (DLTS) and isothermal capacitance transient spectroscopy (ICTS), and resonance methods such as electron spin resonance (ESR) and electron–nuclear double resonance (ENDOR) [25.2].

In the following, we take a-Si:H as an example and describe the nature of its electronic states. Figure 25.6 shows a schematic diagram of the electronic states involved in the band-gap region of a-Si:H proposed by the authors' group [25.9]. The tails of the conduction and valence bands are expressed by an exponential function with widths of 25 meV [25.10] and 48–51 meV [25.11–13], respectively.

In this figure, the processes of radiative recombination and nonradiative recombination are shown, along with the energy levels of the gap states involved in the recombination processes. The radiative recombination occurs between tail electrons and tail holes at higher temperatures and between tail electrons and self-trapped holes (A centres) at lower temperatures, particularly below 60 K. Such recombinations contribute to the principal luminescenceband peaked at 1.3–1.4 eV. These have been elucidated by optically detected magnetic resonance (ODMR) measurements [25.14–16], and are briefly mentioned in Sect. 25.3. The radiative recombination center participating in the low-energy luminescence (defect luminescence) may be attributed to distant $T_3^+-N_2^-$ pair defects [25.17, 18], in which T_3^+ and N_2^- are the positively charged threefold-coordinated silicon center and the negatively charged twofold-coordinated nitrogen center, respectively. The N_2^- centers are created from contaminating nitrogen atoms introduced during sample preparation. On the other hand, close $T_3^+-N_2^-$ pair defects act as nonradiative recombination centers. A typical nonradiative recombination center in a-Si:H is the neutral silicon dangling bond, i. e., T_3^0. The details of the recombination processes in a-Si:H are described in Sect. 25.3.

25.2 Structural Properties

25.2.1 General Aspects

The structural properties of amorphous semiconductors have been investigated by means of X-ray, electron and neutron diffraction, transmission electron microscope (TEM) and scanning electron microscope (SEM), extended X-ray absorption fine structure (EXAFS), small-angle X-ray scattering (SAXS), Raman scattering, infrared absorption (IR) and nuclear magnetic resonance (NMR). The absence of long-range order in amorphous semiconductors is manifested in diffraction techniques, e.g., electron diffraction for a-Si results in a halo pattern as shown in Fig. 25.7a, while Laue spots are seen for c-Si, as shown in Fig. 25.7b. The medium-range order of 0.5–50 nm has been discussed based on SAXS measurements.

25.2.2 a-Si:H and Related Materials

The radial distribution function (RDF) in a-Si has been obtained from an analysis of curves of scattered electron intensity versus scattering angle from electron diffraction measurements, as shown in Fig. 25.8 [25.19]. From a comparison of RDF curves of a-Si and c-Si, it was concluded that the first peak of a-Si coincides with that of c-Si, the second peak of a-Si is broadened compared to that of c-Si, the third peak of c-Si almost disappears and a small peak appears, shifted from the third peak of c-Si, as shown in Fig. 25.8. These results indicate that the bond length of a-Si is elongated by 1% over that of c-Si (= 2.35 Å), and that the bond angle is tetrahedral (= 109.47°) with a variation of 10% from that of c-Si. Using the neutron diffraction technique, the RDF was also deduced from the measured structure factor, $S(Q)$, as a function of Q (the momentum transfer) in a-Si [25.20]. The RDF curve of a-Si exhibiting these features was well simulated by the continuous random network model [25.21]. Since then, computer-generated models have been constructed (see, e.g., *Kugler* et al. [25.20]), using the Monte Carlo (MC) method [25.22], the molecular dynamics (MD) method [25.23] and the reverse MC method [25.24, 25]. Here, the reverse MC method, i. e., a MC simulation repeatedly carried out to reach consistency with the measured RDF curve and curve of structure factor $S(Q)$ versus Q from the neutron diffraction data, is briefly mentioned. First we start with an initial set of Cartesian coordinates (particle configuration) and calculate its RDF and $S(Q)$. Comparing the calculated RDF and $S(Q)$ with the measured ones, the new particle configuration is generated by random motion of a particle, being consistent with the constraint, e.g., the coordination number. From the reverse MC simulation, the bond-angle distribution is derived, i. e., it shows a peak at the tetrahedral angle, 109.5° and small peaks at ≈ 60° and ≈ 90° [25.26].

In a-Si:H, knowledge of the hydrogen configuration is important to understand its electronic properties. This is obtained by NMR [25.27, 28] and IR measurements [25.29]. The bonding modes of Si and H atoms are $Si-H$, $Si-H_2$, $(Si-H_2)_n$ and $Si-H_3$ bonds. The concentrations of these hydrogen configurations depend on the preparation conditions, particularly on the substrate temperature, i. e., the deposition temperature. a-Si:H films prepared at 250 °C mostly contain $Si-H$ bonds in incorporated hydrogen (hydrogen content of ≈ 10 at. %), while those prepared at lower temperatures such as room temperature contain all these bonds in incorporated hydrogen (hydrogen content of

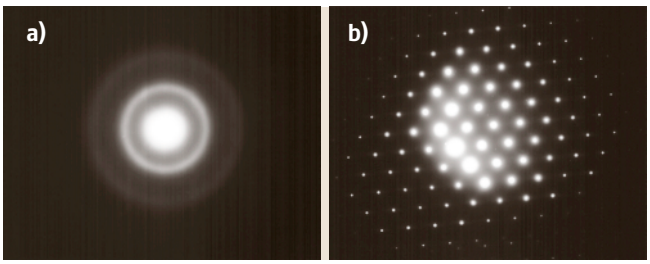

Fig. 25.7a,b Electron diffraction patterns. **(a)** amorphous silicon, **(b)** crystalline silicon

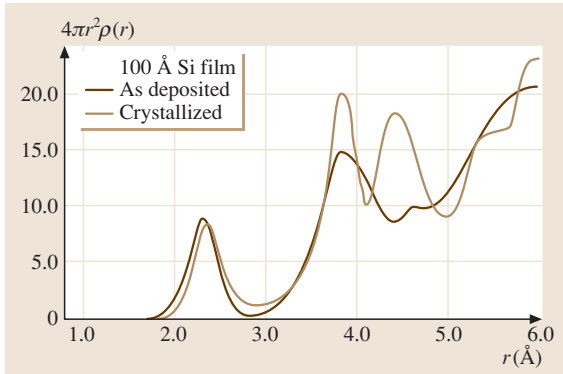

Fig. 25.8 Radial distribution function of amorphous (evaporated) and crystalline silicon obtained from electron diffraction patterns. (After [25.19])

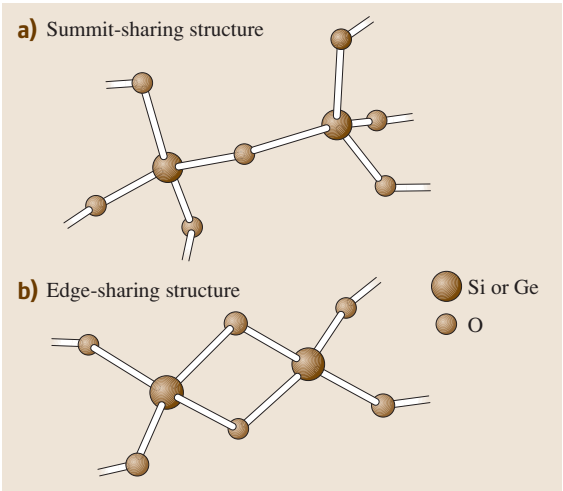

Fig. 25.9a,b Schematic illustration of **(a)** summit-sharing structure and **(b)** edge-sharing structure. (After [25.32])

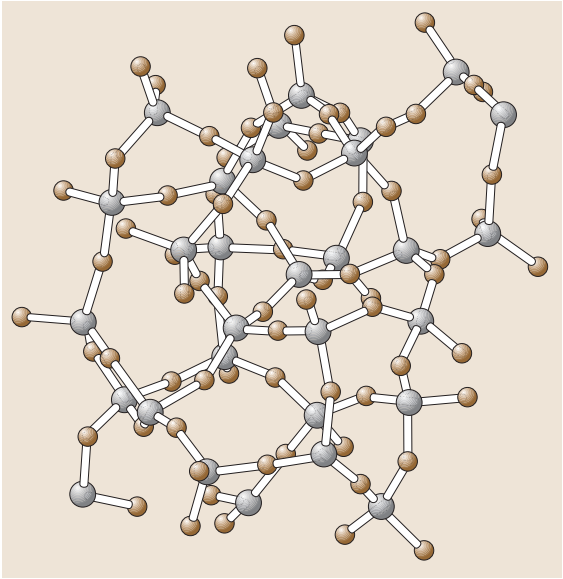

Fig. 25.10 Structural model of germanium disulfide. (After [25.32])

≈ 30 at. %). The hydrogen configuration has also been investigated by neutron scattering measurements using the isotope-substitution method [25.30,31]. Partial pair-correlation functions of Si – Si, Si – H and H – H are obtained from those measurements. The Si–H bond length is 1.48 Å.

Raman scattering measurements provide useful information about microcrystallinity, i. e., the volume fraction of the amorphous phase in microcrystalline silicon [25.33]. The Raman shift associated with transverse optical (TO) phonons is observed at 520 cm^{-1} for c-Si, while it is observed at 480 cm^{-1} for a-Si.

25.2.3 Chalcogenide Glasses

The chalcogenide glasses are composed of chalcogenide atoms and other constituent atoms such as As, Ge etc. Their crystalline counterpart has a structure consisting of threefold-coordinated As atoms and twofold-coordinated chalcogens, i. e., c-Se and c-As_2S_3 exhibit a chain structure and a layered structure, respectively. The structure of the chalcogenide glasses is fundamentally built from these constituent atoms, keeping their coordination in the crystalline counterpart. However, actual glasses contain wrong bonds, i. e., homopolar bonds such as Se–Se, As–As, Ge–Ge etc. In the following, we take two examples of chalcogenide glasses, As_2X_3 (X = S, Se) and GeX_2 (X = S, Se).

1. As_2X_3 (X = S, Se)
   This type of glass, e.g., As_2S_3, is mainly composed of AsS_3 pyramid units, i. e., a random network of these units sharing the twofold-coordinated S site [25.34]. There is no correlation between As atoms, but interlayer correlation seems to hold even for the amorphous structure.
2. GeX_2(X = S, Se)
   Silica glass (SiO_2) is a well-known material, which is mainly composed of SiO_4 tetrahedron units sharing the twofold-coordinated O site (the summit-sharing structure. See Fig. 25.9a). On the other hand, SiS_2 and $GeSe_2$ glasses have a different structure from SiO_2 glass: the tetrahedron units are connected through two X sites (the edge-sharing structure) along with one X site (the summit-sharing structure. See Fig. 25.9b). For example, in $GeSe_2$, the edge-sharing structure occurs at a level of more than 30% and the summit-sharing structure with less than 70%. Actually, wrong bonds (homopolar bonds) Ge–Ge, Se–Se exist in $GeSe_2$ glass. A structural model of GeS_2 [25.32] is shown in Fig. 25.10.

25.3 Optical Properties

25.3.1 General Aspects

Optical absorption and luminescence occur by transition of electrons and holes between electronic states such as conduction and valence bands, tail states, and gap states. In some cases, electron–phonon coupling is strong and, as a result, self-trapping occurs. Exciton formation has also been suggested in some amorphous semiconductors.

The absorption of photons due to interband transition, which occurs in crystalline semiconductors, is also observed in amorphous semiconductors. However, the absorption edge is not clear since interband absorption near the band gap is difficult to distinguish from tail absorption in the absorption spectra. Figure 25.11 schematically illustrates typical absorption spectra of amorphous semiconductors. The absorption coefficient, α, due to interband transition near the band gap is known to be well described by the following equation [25.35]

$$\alpha\hbar\omega = B(\hbar\omega - E_g)^2 \,, \tag{25.1}$$

where $\hbar\omega$ and E_g denote the photon energy and optical gap, respectively. In most amorphous semiconductors, the optical gap E_g is determined by a plot of $(\alpha\hbar\omega)^{1/2}$ versus $\hbar\omega$, which is known as Tauc's plot. The photon energy at which the absorption coefficient is $10^4\,\mathrm{cm}^{-1}$, E_{04}, is also used for the band gap in a-Si:H. The absorption coefficient at the photon energy just below the optical gap (tail absorption) depends exponentially on the photon energy, $E = \hbar\omega$, as expressed by

$$\alpha(E) \propto \exp\left(\frac{E}{E_U}\right) \,, \tag{25.2}$$

where E_U is called the Urbach energy and also the Urbach tail width. In addition, optical absorption by defects appears at energies lower than the optical gap.

Photoluminescence (PL) occurs as a result of the transition of electrons and holes from excited states to the ground state. After interband excitation, electrons relax to the bottom of the conduction band by emitting phonons much more quickly than the radiative transition. Similarly, the holes also relax to the top of the valence band. In the case of crystalline semiconductors without defects or impurities, there is no localized state in the band gap and PL occurs by transition between the bottom of the conduction band and the top of the valence band. In this case the k-selection rule, $k_{photon} = k_i - k_f$, must be satisfied, where k_{photon}, k_i and k_f denote the wavenumbers of photons, and electrons in the initial and final states, respectively. Since k_{photon} is much smaller than k_i and k_f, we can rewrite the selection rule as $k_i = k_f$. Semiconductors satisfying this condition are called direct-gap semiconductors. Crystalline silicon is one semiconductor in which the direct transition is not allowed by the k-selection rule (indirect-gap semiconductors), but the transition is allowed by either absorption of phonons or their emission. On the other hand, strong PL is observed in a-Si:H. In amorphous semiconductors, the k-selection rule is relaxed and, furthermore, the electrons and holes relax to localized states in the gap before radiative recombination. Thus, PL occurs by transitions between localized states.

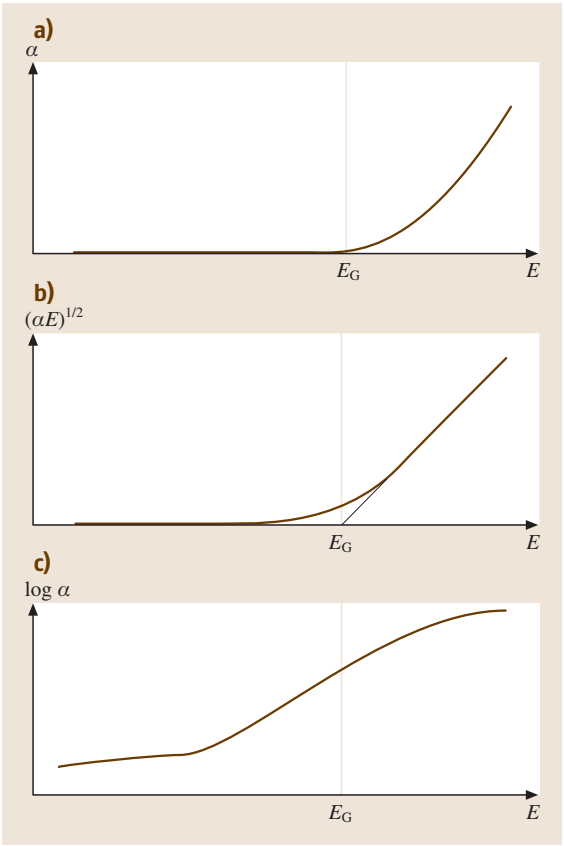

Fig. 25.11a–c Schematic illustration of the absorption spectra of amorphous semiconductors. **(a)** The absorption coefficient α plotted as a function of photon energy E. **(b)** $(\alpha E)^{1/2}$ versus E (Tauc's plot). **(c)** $\log\alpha$ versus E. E_G is the optical gap determined from (b)

The lifetime measurement is important for the identification of the origin of the PL since the PL spectra in most amorphous semiconductors are featureless and do not provide much information. The probability of radiative transition between localized electrons and holes depends exponentially on their separation, R. The lifetime is estimated by $\tau = \tau_0 \exp(2R/R_0)$ where R_0 denotes the radius of the most extended wavefunction [25.36]. When the Coulomb interaction is strong enough, excitons are formed. Exciton formation is also suggested in some amorphous semiconductors. The total spin of excitons, S, is either 0 or 1. Singlet excitons of $S = 0$ have a lifetime in the nanosecond region, while triplet excitons with $S = 1$ have a lifetime much longer than that of singlet excitons, e.g. $\tau = 1$ ms, since the transition is forbidden by the spin selection rule.

PL measurements combined with magnetic resonance are a powerful means to study recombination processes [25.14, 15]. This is called optically detected magnetic resonance (ODMR) measurements. PL from triplet excitons has been suggested from ODMR measurements, as described in Sects. 25.3.2 and 25.3.3.

The photoconductivity measurements provide us with useful information about the processes of carrier transport and recombination. Their results on a-Si:H and chalcogenide glasses are briefly reviewed in Sects. 25.3.2 and 25.3.3, respectively.

Table 25.1 Optical gap of a-Si:H prepared at various deposition temperatures

T_s (°C)	[H] (at.%)	E_g (eV)	References
300	7	1.70	[25.37, 38]
200	18	1.75	[25.37, 38]
120	28	1.9	[25.37, 38]
75	33	2.0	[25.38, 39]

T_s: Deposition temperature, [H]: Hydrogen content

25.3.2 a-Si:H and Related Materials

The band gap of a-Si:H determined from Tauc's plot is 1.7–1.9 eV, depending on the preparation condition, particularly the deposition temperature, T_s, i. e. hydrogen content, [H], [25.37–39, 48] as shown in Table 25.1. The absorption coefficient of visible light for a-Si:H is of the order 10^5–10^6 cm^{-1}, which is large compared to that of crystalline silicon. A thickness of 1 μm is enough to absorb visible light. Thus a-Si:H is suitable for application to solar cells especially when a thin film is desired.

The optical gap, E_g, and the Urbach tail width, E_U, of a-Si:H, a-Ge:H and Si-based alloys are shown in Table 25.2. Some a-Si:H-based alloys such as a-$Si_{1-x}N_x$:H and a-$Si_{1-x}C_x$:H have a band gap wider than that of a-Si:H depending on the composition, x. In the preparation of these alloys, x can be varied continuously over a certain range. Thus, the band gap can be varied arbitrarily. It is possible to prepare multilayer films consisting of layers with different band gaps, such as a-Si:H/a-$Si_{1-x}N_x$:H. Quantum size effects in multilayer films will be described in Sect. 25.6.

It is difficult to obtain the absorption spectra below the band gap from transmittance measurements in a-Si:H, which is normally prepared as a thin film. Such low absorption in a-Si:H has been measured by PDS and CPM.

PL from a-Si:H was observed by Engemann and Fischer [25.49] for the first time. The quantum efficiency has been found to be of the order of unity [25.50], although it decreases with increasing density of dangling bonds [25.51]. PL spectra from a-Si:H films generally consist of two components. The first is observed as a peak at 1.3–1.4 eV with a FWHM of 0.3 eV. The other component, which is called low-energy PL (defect PL), is observed at 0.8–0.9 eV.

The origin of the main peak has not been fully understood. Electrons and holes in the tail states may give

Table 25.2 Band gap energies, Urbach tail widths and dark conductivities at room temperature for a-Si:H, a-Ge:H and related materials

Material	E_g (eV)	E_U (meV)	σ(300 K) (Ω^{-1}cm^{-1})	References
a-Si:H	1.75	48	10^{-11}	[25.40, 41]
a-Ge:H	1.05	50	10^{-4}	[25.40, 41]
a-$Si_{0.7}C_{0.3}$:H	2.28	183.4		[25.42]
a-$Si_{0.8}C_{0.2}$:H	2.2		10^{-15}	[25.43]
a-$Si_{0.4}N_{0.6}$:H	3.0	≈ 200	≈ 10^{-8}	[25.44–46]
a-$Si_{0.74}N_{0.26}$:H	≈ 2.0	≈ 100	1.4×10^{-8}	[25.44, 45, 47]

rise to this PL. Dunstan and Boulitrop [25.52] have shown that the PL spectra of a-Si:H can be understood without considering electron–phonon coupling. However, the electron–phonon coupling has still been discussed. Morigaki proposed a model on the basis of ODMR measurements [25.14] in which self-trapped holes and tail electrons are the origin of the PL at low temperatures [25.53], while tail holes and tail electrons participate in the PL at high temperatures.

In the case of radiative recombination of localized electron–hole pairs the lifetime depends exponentially on the separation of the electron and the hole, as described in Sect. 25.3.1. When the spatial distribution of electrons and holes is random, a broad lifetime distribution is predicted. This model describes some properties well, e.g., the generation-rate dependence of the lifetime. However, it has been pointed out that we have to consider the PL from specific electronic states such as excitonic PL to understand the lifetime distribution at low generation rate [25.54–56]. PL due to triplet excitons in a-Si:H has been suggested by optically detected magnetic resonance measurements [25.57, 58]. The PL from singlet excitons, which is expected to have lifetime of about 10 ns, has also been reported [25.59–61].

The low-energy PL is emission from deep gap states created by defects. However the origin of low-energy PL is not neutral dangling bonds (T_3^0) of Si since they act as nonradiative centers, as has been suggested from optically detected magnetic resonance [25.62]. *Yamaguchi* et al. [25.17, 18] proposed a model in which the origin of the low-energy PL is $T_3^+ - N_2^-$ pairs.

The drift mobility of carriers, i. e., electrons and holes, in a-Si:H has been measured by the method of time of flight (TOF), using blocking electrodes [25.63]. In the measurement, carriers are created by an optical pulse near one of the electrodes and run as a sheet-like shape against another electrode. The transient photocurrent i_p associated with a pulsed optical excitation exhibits a dispersive behavior, as shown in Fig. 25.12 [25.63, 64], which is given by

$$i_p \propto t^{-(1-\alpha)} \quad \text{for} \quad t < t_r \tag{25.3}$$

and

$$i_p \propto t^{-(1+\alpha)} \quad \text{for} \quad t > t_r \,, \tag{25.4}$$

where t_r designates the transit time, as shown in Fig. 25.12, given by

$$t_r = \frac{L}{\mu_d F} \,, \tag{25.5}$$

in which L, μ_d and F are the separation of the two electrodes, the drift mobility and the magnitude of the electric field, respectively. In dispersive conduction, the drift mobility depends on the thickness of the samples. This is due to dispersive carrier processes, which are caused by dispersion of the flight time. Band conduction with multiple trapping of carriers also exhibits dispersive conduction, as was observed in a-Si:H and chalcogenide glasses. For undoped a-Si:H, the drift mobility was on the order of $1\,\mathrm{cm^2/V}$ at room temperature. $\alpha = 0.51$ was obtained as 160 K [25.11]. This transient behavior depends on temperature, i. e., it becomes more dispersive at lower temperatures. α is related to the exponential tail width (normally equal to E_U) $E_c \equiv k_B T_c$ as follows:

$$\alpha = \frac{T}{T_c} \,. \tag{25.6}$$

From the value of α, the tail width of the conduction band has been obtained to be 25 meV. For hole transport, dispersive behavior has also been obtained and a drift mobility of the order of $10^{-2}\,\mathrm{cm^2/V}$ has been obtained at room temperature.

For the steady-state photoconductivity of undoped a-Si:H, it has been generally accepted that photoconduction occurs through electrons in the conduction band at temperatures above ≈ 60 K and through hopping of tail electrons at temperatures below ≈ 60 K. The detailed processes of trapping and recombination of carriers involved in photoconduction have been discussed in many literatures (see, e.g., *Morigaki* [25.2]; *Singh* and *Shimakawa* [25.3]). In relation to this issue, spin-dependent photoconductivity measurements are very useful, and have therefore been extensively performed on a-Si:H [25.65–67].

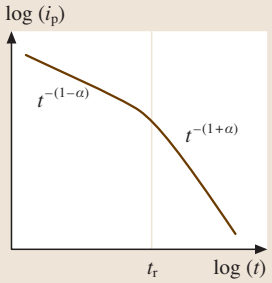

Fig. 25.12 Schematic illustration of the transient photocurrent curve for the dispersive transport

25.3.3 Chalcogenide Glasses

As mentioned in Sect. 25.3.1, the absorption coefficient for the interband transition in many chalcogenide

Table 25.3 Band gap energies, drift mobilities, and dark conductivities at room temperature for chalcogenide glasses [25.2]

Material	E_g [25.68] (eV)	μ_d (cm^2/Vs) [25.1, 69] n-type	p-type	σ (300 K) [25.68] ($\Omega^{-1}cm^{-1}$)
Se	2.05	$3-6\times10^{-3}$	$1-2\times10^{-1}$	10^{-16}
As_2S_3	2.32			10^{-17}
As_2Se_3	1.76		10^{-3}	10^{-12}
As_2Te_3	0.83		10^{-2}	10^{-4}
GeS_2	3.07			10^{-14}
$GeSe_2$	2.18	1.4×10^{-1}	4×10^{-2}	10^{-11}
Sb_2Se_3	0.70			
Cd – In – S [25.70]	2.2	30 *)		9×10^{-1}

*) Hall mobility

glasses is well described by Tauc's relationship (25.1). The optical gap E_g is shown in Table 25.3 for various chalcogenide glasses. The effect of light on optical absorption in chalcogenide glasses is known as photo-darkening. This effect will be briefly reviewed in Sect. 25.5.

PL has been observed in a-Se, arsenic chalcogenide glasses and germanium chalcogenide glasses. PL in chalcogenide glasses is known to have a large Stokes shift. The peak energy in the PL spectra is approximately half of the band gap. This stokes shift has been attributed to strong electron–phonon coupling [25.71]. The electronic states responsible for the PL have not been well understood. There has been some experimental evidence for PL from self-trapped excitons. The observation of triplet excitons has been reported in ODMR measurements for chalcogenide glasses such as As_2S_3 and As_2Se_3 [25.72–74].

Dispersive transport was observed in the transient photocurrent for the first time for chalcogenide glasses such as a-As_2Se_3, in which the hole transport dominates over the electron transport [25.63]. The drift mobility of holes ranges between 10^{-3}–10^{-5} cm^2/V, depending on the temperature and electric field. The zero-field hole mobility at room temperature is about 5×10^{-5} cm^2/V. The steady-state photoconduction in a-As_2Se_3 has been considered to be governed by charged structural defects such as VAPs.

25.4 Electrical Properties

25.4.1 General Aspects

Electrical Conductivity

Electrical conduction in amorphous semiconductors consists of band conduction and hopping conduction. Band conduction in undoped amorphous semiconductors is characterized by

$$\sigma = \sigma_0 \exp\left(-\frac{E_a}{k_B T}\right), \tag{25.7}$$

where σ and σ_0 are the electrical conductivity and a prefactor, respectively, and E_a, k_B and T are the activation energy, the Boltzmann constant and the temperature, respectively. E_a is given by either $E_c - E_F$ or $E_F - E_V$, depending on whether electrons or holes are considered, where E_c, E_V and E_F are the mobility edges of the conduction band and the valence band, and the Fermi energy, respectively. Hopping conduction in amorphous semiconductors consists of nearest-neighbor hopping and variable-range hopping [25.1]. Nearest-neighbor hopping is well known in crystalline semiconductors, in which electrons (holes) hop to nearest-neighbor sites by emitting or absorbing phonons. Variable-range hopping is particularly associated with tail states, in which electrons (holes) in tail states hop to the most probable sites. This type of hopping conductivity σ_p is characterized by the following temperature variation:

$$\sigma_p = \sigma_{p0} \exp\left(-\frac{B}{T^{1/4}}\right). \tag{25.8}$$

The Hall Effect

The Hall effect is used for the determination of carrier density and its sign in crystalline semiconductors. For amorphous semiconductors, however, the sign of the Hall coefficient does not always coincide with that of the carriers [25.76]. Such a sign anomaly has been observed in a-Si:H, as will be shown in Sect. 25.4.2.

Thermoelectric Power

The thermoelectric power S associated with band conduction of electrons is given by

$$S = -\frac{k_B}{e}\left(\frac{E_c - E_F}{k_B T} + A\right) , \tag{25.9}$$

where A is a quantity depending on the energy dependence of the relaxation times associated with electrical conduction. For hole conduction, S is given by (25.9) except that $E_c - E_F$ is replaced by $E_F - E_V$ and that the sign of S is positive. The sign of S coincides with that of the carriers. The thermoelectric power S (25.9) is related to the electrical conductivity σ (25.7) as follows [25.77]:

$$\ln\sigma + \left|\frac{e}{k_B}S\right| = \ln\sigma_0 + A \equiv Q . \tag{25.10}$$

The temperature-dependent quantity Q is defined as above. The activation energies of σ and S, E_σ and E_S, are equal to each other. Then, Q is defined by Q_0 as follows:

$$Q = \ln\sigma_0 + A \equiv Q_0 . \tag{25.11}$$

However, if E_σ is not equal to E_S, Q is generally expressed by

$$Q = Q_0 - \frac{E_Q}{k_B T} \tag{25.12}$$

$$E_Q = E_\sigma - E_S . \tag{25.13}$$

It has been generally observed that E_σ is greater than E_S, i. e., $E_\sigma > E_S$. This has been accounted for in terms of long-range fluctuation of the band edge. The electrical conduction is due to those carriers that are thermally excited into the valley of the band-edge fluctuation and cross over its barrier, while the thermoelectric power, i. e., transport of phonon energy by carriers, is governed by carriers in the valleys. Thus, a relationship of $E_\sigma > E_S$ can be accounted for in terms of long-range fluctuation of the band edge [25.77].

Drift Mobility

The drift mobility of carriers is measured by the TOF method, as mentioned in Sect. 25.3.2. The drift mobility μ_d is estimated from (25.5).

In the following, the electrical properties of a-Si:H and related materials and chalcogenide glasses are described.

25.4.2 a-Si:H and Related Materials

A typical example of band conduction and variable-range hopping conduction is shown in Fig. 25.13, which is the temperature dependence of the electrical conductivity for a-Si_xAu_{1-x} films prepared by vapor evaporation [25.75]. Band conduction occurs at high temperatures and variable-range hopping conduction at low temperatures. The $T^{-1/4}$ law of temperature variation of electrical conductivity is clearly seen in Fig. 25.14. The values of the dark conductivities of a-Si:H, a-Ge:H and related materials at room temperature are shown in Table 25.2. Figure 25.15 shows the temperature dependencies of S for a-Ge:H, in which two slopes of the curve of S versus T^{-1} are seen with 0.43 eV in the high-temperature range and 0.17 eV in the low-temperature range [25.78]. This crossover of two slopes is accounted for in terms of two different mechanisms of electrical conduction, i. e., band conduction at high temperatures and hopping conduction in the band-tail states at low temperatures [25.79]. In amorphous semiconductors, doping control is generally difficult, because the constituent

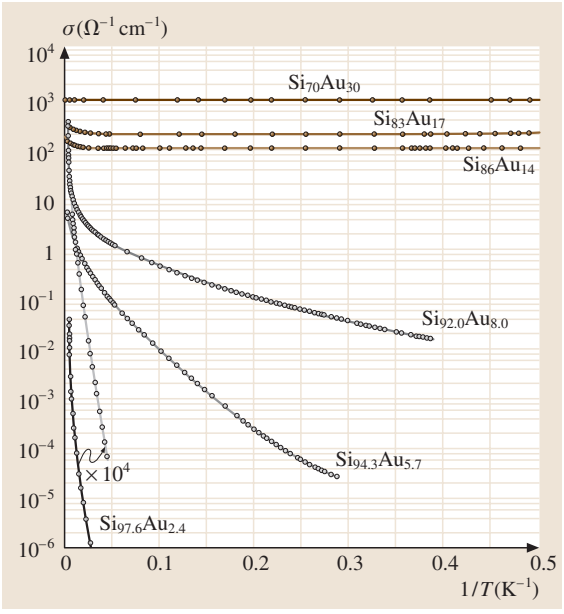

Fig. 25.13 Temperature dependence of the electrical conductivity for an a-Si_xAu_{1-x} film. (After [25.75])

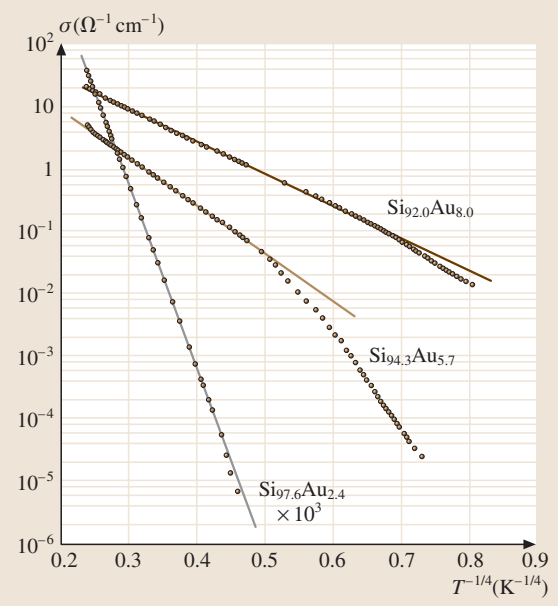

Fig. 25.14 Electrical conductivity versus $T^{-1/4}$ for a-Si_xAu_{1-x} films. (After [25.75])

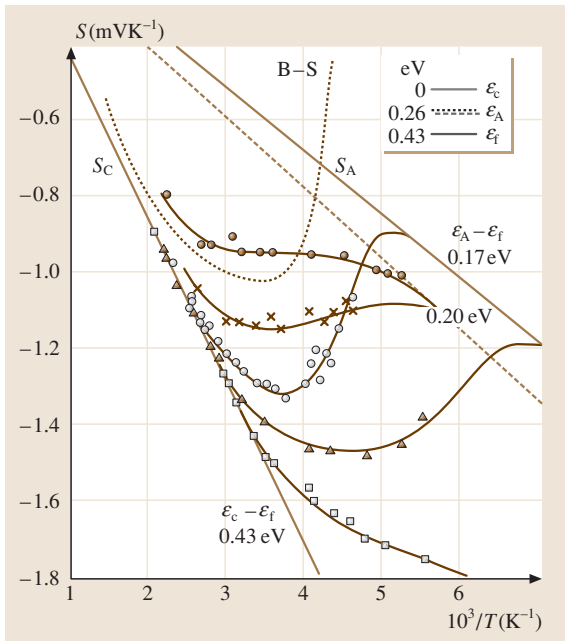

Fig. 25.15 Thermoelectric power versus T^{-1} for various a-Ge:H films. The *solid lines* are the calculated results. The *insert* shows the model on which the calculations are based. Carriers in states just above E_A move in extended states, those at E_A move by hopping. The *dotted curve* marked B–S was obtained by *Beyer* and *Stuke* [25.81] for a slowly evaporated sample annealed at 310 °C [25.78]

atoms obey the so called $8-N$ rule to satisfy the coordination of covalent bonds with their neighboring atoms. In a-Si:H, however, n-type doping and p-type doping were performed by using phosphorus (group V element) and boron (group III element), respectively [25.80].

The Hall coefficient of a-Si:H has been measured [25.76]. In crystalline semiconductors, when the carriers are electrons, its sign is negative, and when the carriers are holes, its sign is positive. The sign of the Hall coefficient is generally negative irrespective of that of the carriers in amorphous semiconductors. This has been accounted for in terms of the random phase model [25.82]. However, for the Hall coefficient of a-Si:H, this is not the case, i. e., when the carriers are electrons, the sign is positive, and when the carriers are holes, the sign is negative. Such an anomalous Hall coefficient in a-Si:H is called double reversal of the Hall coefficient and has been accounted for, taking into account antibonding orbitals for electrons and bonding orbitals for holes [25.83].

25.4.3 Chalcogenide Glasses

The values of the dark conductivities of chalcogenide glasses at room temperature are shown in Table 25.3 along with those of μ_d at room temperature. In chalcogenide glasses, the Fermi level is pinned near the midgap and this has been considered to be due to VAP defects with negative correlation energy. Thus, doping seems difficult, except for a few cases, e.g., the incorporation of Bi into a-Ge:S and a-Ge:Se increases the direct current (DC) conductivity by 6–7 orders of magnitude [25.84, 85]. This doping effect is due to chemical modification instead of conventional doping. Furthermore, Cd–In–S chalcogenide glasses exhibit $\sigma \approx 1\times10^{-2}\,\Omega^{-1}\mathrm{cm}^{-1}$ at room temperature [25.70].

25.5 Light-Induced Phenomena

Light-induced phenomena in amorphous semiconductors were first observed for chalcogenide glasses as photo-darkening, PL fatigue and photostructural changes associated with illumination whose energy

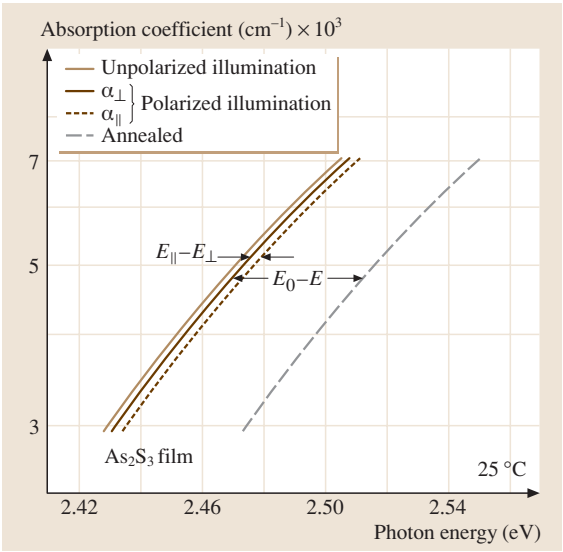

Fig. 25.16 Optical absorption edge of As_2S_3 films annealed or illuminated with unpolarized or linearly polarized light ($\alpha_\perp$: *solid line* and $\alpha_{||}$: *dashed line*). $\alpha_{||}$ and $\alpha_\perp$ refer to polarization along the plane of illumination and perpendicular to it, respectively. (After [25.87])

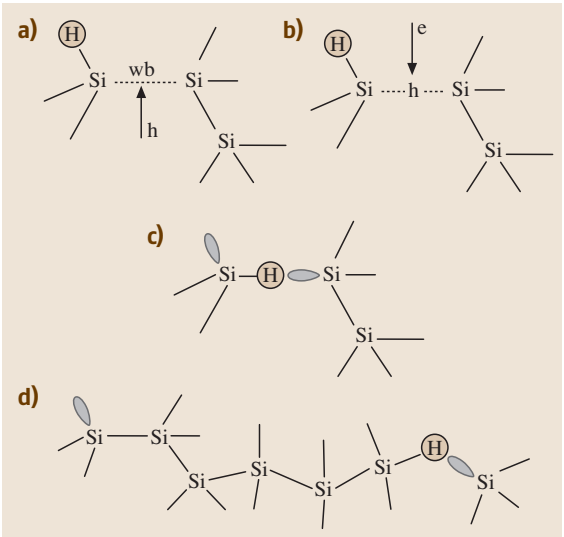

Fig. 25.17 **(a)** Self-trapping of a hole by a weak Si – Si bond adjacent to a Si – H bond. **(b)** Nonradiative recombination of a self-trapped hole with an electron. **(c)** A Si – H bond is switched toward the weak Si – Si bond and a dangling bond is left behind. **(d)** Formation of two separate dangling bonds after hydrogen movements and repeating of processes shown in **(a)–(c)**

equals to or exceeds the band-gap energy (see, e.g., Shimakawa et al. [25.86]; Singh and Shimakawa, [25.3]). Photo-darkening is an effect in which the absorption edge shifts towards lower photon energy under illumination, as shown in Fig. 25.16 [25.87]. PL fatique is the decrease of the PL intensity associated with illumination. Photostructural changes are observed as changes of the volume (generally expansion) of the sample with illumination. PL fatigue may be due to light-induced creation of charged structural defects acting as nonradiative recombination centers. For the photo-darkening and the photostructural change, it has been discussed whether they are independent of each other or not. Thus, the origins of these phenomena are still unclear.

Light-induced phenomena in a-Si:H were observed first in the dark conductivity and photoconductivity, i. e., drops in their values after prolonged illumination of band-gap light (the so-called Staebler–Wronski effect [25.88]). Subsequently, such phenomena have been observed in PL, optical absorption and ODMR etc. [25.2]. This effect also gives rise to degradation of the performance of amorphous-silicon solar cells, so that this has received great attention from the viewpoint of application. After prolonged illumination, dangling bonds were found to be created [25.89, 90], so that light-induced creation of dangling bonds has been considered as the origin of these phenomena. Several models have been proposed for mechanisms for light-induced creation of dangling bonds [25.53, 91–96], but this issue is still controversial (see, e.g., *Morigaki* [25.2]; *Singh* and *Shimakawa* [25.3]). Very recently, the creation of a number of dangling bonds such as 1×10^{19} cm^{-3} after pulsed optical excitation has been observed in high-quality a-Si:H films [25.97, 98]. This result has been accounted for in terms of the authors' model [25.99], based on a combination of the following processes occurring during illumination. Self-trapping of holes in weak Si – Si bonds adjacent to Si – H bonds triggers these weak bonds to break using the phonon energy associated with nonradiative recombination of electrons with those self-trapped holes (Fig. 25.17a and b). After Si – H bond switching and hydrogen movement, two types of dangling bonds are created, i. e., a normal dangling bond and a dangling bond with hydrogen at a nearby site, i. e. so-called hydrogen-related dangling bonds (Fig. 25.17c and d). In the latter, hydrogen is dissociated from the Si – H bond as a result of nonradiative recombination at this dangling bond site. Dissociated hydrogen can terminate two types of dangling bonds (Fig. 25.18c and d) or can be in-

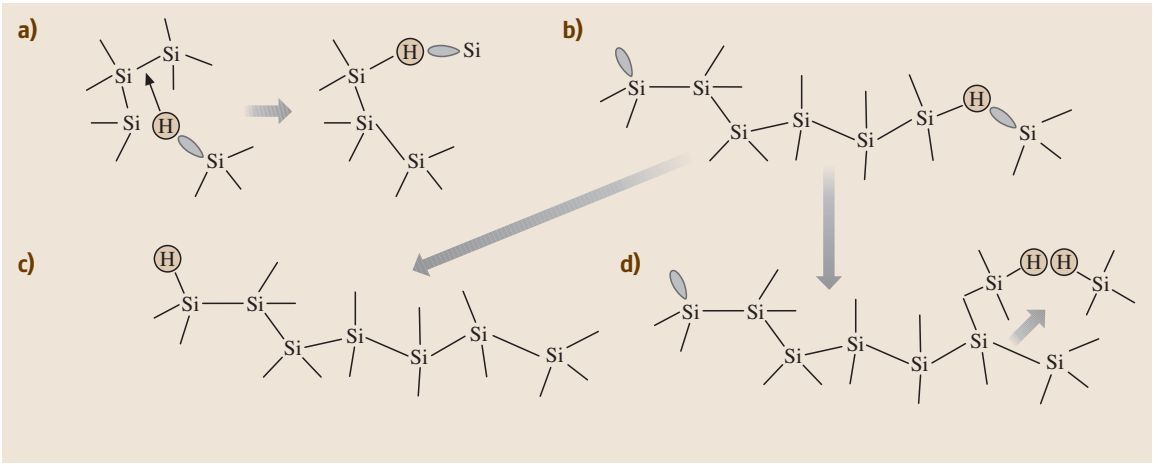

Fig. 25.18 **(a)** Dissociation of hydrogen from a hydrogen-related dangling bond and insertion of hydrogen into a nearby weak Si – Si bond (formation of a new hydrogen-related dangling bond). **(b)** Two separate dangling bonds, i. e. a normal dangling bond and a hydrogen-related dangling bond. **(c)** Dissociation of hydrogen from a hydrogen-related dangling bond and termination of a normal dangling bond by hydrogen. **(d)** Termination of a hydrogen-related dangling bond by hydrogen

serted into a nearby weak Si – Si bond (Fig. 25.18a). The dependencies of the density of light-induced dangling bonds on illumination time and generation rate have been calculated using the rate equations governing these processes. The results have been compared with experimental results obtained under continuous illumination and pulsed illumination with good agreement. Light-induced structural changes, i. e., volume change [25.100] and local structural changes around a Si – H bond [25.101] have also been observed in a-Si:H and the origins for these changes have been discussed [25.102–104].

25.6 Nanosized Amorphous Structure

Recent technologies have enabled us to control the properties of semiconductors by introducing artificial structures of nanometer size such as quantum wells, quantum wires and quantum dots. The quantum well is formed by preparing multilayers consisting of two semiconductors. Figure 25.19a illustrates the conduction and valence band edges in such multilayers consisting of two semiconducting materials with different band gaps, plotted as functions of the distance from the substrate, z. The curves of the conduction and valence bands in Fig. 25.19a are considered to be the potentials for the electrons and holes, respectively. The motion of the electrons and holes is assumed to be described by effective mass equations which are similar to the Schrödinger equation. When the barriers of the potentials are high enough to prevent the carriers from moving to the adjacent well, the quantum levels (for motion along the z-axis) are as illustrated in Fig. 25.19a. The band gap of the multilayer, E_g, is equal to the separation of the quantum levels of the lowest energy in the conduction and valence bands, as shown in Fig. 25.19a. E_g increases with decreasing thickness of the well layer, L_w; this is well known as the quantum-size effect. When the height of the barrier is infinite, $\Delta E = E_g - E_{gw}$ is proportional to L_w^{-2}, where E_{gw} denotes the band gap of the material of the well layer.

Multilayers of various amorphous semiconductors have been prepared. Observation of the quantum size effect has been reported in some amorphous semiconducting multilayers. For example, the shift of the optical gap of an a-Si:H/a-$Si_{1-x}N_x$:H multilayer from that of a-Si:H, ΔE, is proportional to L_w^{-2}, where L_w is the thickness of the a-Si:H layers (e.g. Morigaki [25.2]; see Yamaguchi and Morigaki [25.105]; and references therein). The result, $\Delta E \propto L_w^{-2}$, is consistent with quantum size effect in a square-well potential.

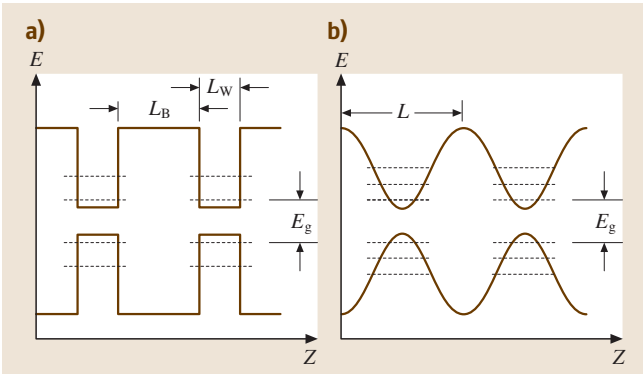

Fig. 25.19a,b The edges of the conduction and valence bands in **(a)** multilayer films and **(b)** band-edge modulated films, as functions of z, where z denotes distance from the substrates. The *dashed lines* indicate quantum levels. The band gap E_g, which increases due to the quantum size effect, is also shown

In the case of amorphous semiconductors, it is easy to introduce a potential well of arbitrary shape, because the optical gap of the amorphous semiconducting alloy, which depends on the composition, can be varied continuously within a certain range. The authors have prepared a new type of a-Si:H-based film called band-edge modulated (BM) a-$Si_{1-x}N_x$:H, in which the potentials for electrons and holes are sinusoidal functions of z [25.106,107]. The band-edges for the BM films are illustrated in Fig. 25.19b. In this case, the quantum size effect is also expected, similarly to the case of multilayer films. However, the quantum levels and the size dependencies of the band gap are different from those in the case of multilayer films. In the case of BM, the potential is approximately parabolic at the bottom of the well. In this case the quantum levels have the same separation as that illustrated in Fig. 25.19b. We expect that the shift of the optical gap in BM films, ΔE, will be proportional to L^{-1}, where L denotes the modulation period. The band gap of BM films observed in experiments are in agreement with that expected from the above consideration [25.106]. Parabolic potentials in crystalline semiconductors have also been introduced (see Gossard et al. [25.108]). However it is difficult to obtain such structures that are small enough to observe significant quantum effects in crystalline semiconductors.

Recently, preparation of amorphous silicon quantum dots in silicon nitride has been reported [25.109]. Theoretical calculations for silicon nanostructures [25.110] have predicted that the oscillator strength in low symmetry is larger than that in high symmetry. A large quantum efficiency for PL is expected in the case of amorphous quantum dots. Thus, amorphous quantum wires and dots have potential applications in light-emitting devices with high efficiency.

Chalcogenide glasses multilayers have been prepared [25.111–113], whose optical properties such as optical absorption and PL, and electrical properties have been measured.

References

25.1 N. F. Mott, E. A. Davis: *Electronic Processes in Non-crystalline Materials*, 2nd edn. (Clarendon, Oxford 1979)

25.2 K. Morigaki: *Physics of Amorphous Semiconductors* (World Scientific, Singapore; Imperial College Press, London 1999)

25.3 J. Singh, K. Shimakawa: *Advances in Amorphous Semiconductors* (Taylor Francis, London 2003)

25.4 S. Kugler, P. R. Surján, G. Náray-Szabó: Phys. Rev. B **37**, 9069 (1988)

25.5 L. Ley, J. Reichardt, R. L. Johnson: Phys. Rev. Lett. **49**, 1664 (1982)

25.6 L. Brey, C. Tejedor, J. A. Verges: Phys. Rev. Lett. **52**, 1840 (1984)

25.7 L. Ley, S. Kawalczyk, R. Pollak, D. A. Shirley: Phys. Rev. Lett. **29**, 1088 (1972)

25.8 M. Kastner, D. Adler, H. Fritzsche: Phys. Rev. Lett. **37**, 1504 (1976)

25.9 K. Morigaki, M. Yamaguchi, I. Hirabayashi, R. Hayashi: *Disordered Semiconductors*, ed. by M. A. Kastner, G. A. Thomas, S. R. Ovshinsky (Plenum, New York 1987) p. 415

25.10 G. D. Cody: In: *Semiconductors and Semimetals*, Vol. 21, Part B ed. by J. I. Pankove (Academic, Orlando 1984) p. 1

25.11 T. Tiedje: In: *Semiconductors and Semimetals*, Vol. 21, Part C ed. by J. I. Pankove (Academic, Orlando 1984) p. 207

25.12 K. Winer, I. Hirabayashi, L. Ley: Phys. Rev. B **38**, 7680 (1988)

25.13 K. Winer, I. Hirabayashi, L. Ley: Phys. Rev. Lett. **60**, 2697 (1988)

25.14 K. Morigaki: In: *Semiconductors and Semimetals*, Vol. 21, Part C ed. by J. I. Pankove (Academic, Orlando 1984) p. 155

25.15 K. Morigaki, M. Kondo: Solid State Phenomena **44-46**, 731 (1995)

25.16 K. Morigaki, H. Hikita, M. Kondo: J. Non-Cryst. Solids **190**, 38 (1995)

25.17 M. Yamaguchi, K. Morigaki, S. Nitta: J. Phys. Soc. Jpn. **58**, 3828 (1989)
25.18 M. Yamaguchi, K. Morigaki, S. Nitta: J. Phys. Soc. Jpn. **60**, 1769 (1991)
25.19 S. C. Moss, J. F. Graczyk: *Proc. 10th Int. Conf. on Physics of Semiconductors*, ed. by J. C. Hensel, F. Stern (US AEC Div. Tech. Inform., Springfield 1970) p. 658
25.20 S. Kugler, G. Molnár, G. Petö, E. Zsoldos, L. Rosta, A. Menelle, R. Bellissent: Phys. Rev. B **40**, 8030 (1989)
25.21 D. E. Polk: J. Non-Cryst. Solids **5**, 365 (1971)
25.22 F. Wooten, K. Winer, D. Weaire: Phys. Rev. Lett. **54**, 1392 (1985)
25.23 R. Car, M. Parrinello: Phys. Rev. Lett. **60**, 204 (1988)
25.24 S. Kugler, L. Pusztai, L. Rosta, P. Chieux, R. Bellissent: Phys. Rev. B **48**, 7685 (1993)
25.25 L. Pusztai: J. Non-Cryst. Solids **227–230**, 88 (1998)
25.26 S. Kugler, K. Kohary, K. Kádas, L. Pusztai: Solid State Commun. **127**, 305 (2003)
25.27 J. A. Reimer: J. Phys. (Paris) **42**, C4–715 (1981)
25.28 K. K. Gleason, M. A. Petrich, J. A. Reimer: Phys. Rev. B **36**, 3259 (1987)
25.29 G. Lucovsky, R. J. Nemanich, J. C. Knights: Phys. Rev. B **19**, 2064 (1979)
25.30 R. Bellissent, A. Menelle, W. S. Howells, A. C. Wright, T. M. Brunier, R. N. Sinclair, F. Jansen: Physica B **156, 157**, 217 (1989)
25.31 A. Menelle: Thése Doctorat (Université Piere et Marie Curie, Paris 1987)
25.32 T. Uchino: Kotai Butsuri (Solid State Physics) **37**, 965 (2002)
25.33 J. H. Zhou, K. Ikuta, T. Yasuda, T. Umeda, S. Yamasaki, K. Tanaka: J. Non-Cryst. Solids **227–230**, 857 (1998)
25.34 G. Lucovsky, F. L. Galeener, R. H. Geils, R. C. Keezer: In: *Proc. Int. Conf. on Amorphous and Liquid Semiconductors*, ed. by W. E. Spear (University of Edinburgh, Edinburgh 1977) p. 127
25.35 J. Tauc: In: *Amorphous and Liquid Semiconductors*, ed. by J. Tauc (Plenum, New York 1974) p. 159
25.36 C. Tsang, R. A. Street: Phys. Rev. B **19**, 3027 (1979)
25.37 K. Morigaki, Y. Sano, I. Hirabayashi: J. Phys. Soc. Jpn. **51**, 147 (1982)
25.38 K. Morigaki, Y. Sano, I. Hirabayashi: *Amorphous Semiconductor Technologies and Devices—1983*, ed. by Y. Hamakawa (Ohomsha, Tokio 1983) Chap. 3.2
25.39 I. Hirabayashi, K. Morigaki, M. Yoshida: Sol. Ener. Mat. **8**, 153 (1982)
25.40 G. H. Bauer: Solid State Phenomena **44–46**, 365 (1995)
25.41 W. Paul: In: *Amorphous Silicon and Related Materials*, ed. by H. Fritzsche (World Scientific, Singapore 1989) p. 63
25.42 Y. Tawada: In: *Amorphous Semiconductors—Technologies and Devices*, ed. by Y. Hamakawa (Ohmusha and North Holland, Tokyo and Amsterdam 1983) Chap. 4.2
25.43 F. Demichelis, C. F. Pirri: Solid State Phenomena **44–46**, 385 (1995)
25.44 K. Maeda, I. Umezu: J. Appl. Phys. **70**, 2745 (1991)
25.45 M. Yamaguchi, K. Morigaki unpublished
25.46 B. Dunnett, D. I. Jones, A. D. Stewart: Philos. Mag. B **53**, 159 (1986)
25.47 M. Hirose: Jpn. J. Appl. Phys. **21**(suppl. 21-1), 297 (1981)
25.48 M. Yamaguchi, K. Morigaki: Philos. Mag. B **79**, 387 (1999)
25.49 D. Engemann, R. Fischer: In: *Amorphous and Liquid Semiconductors*, ed. by J. Stuke, W. Brenig (Taylor & Francis, London 1974) p. 947
25.50 D. Engemann, R. Fischer: In: *Proceedings of the 12th International Conference on the Physics of Semiconductors*, ed. by M. H. Pilkuhn (B. G. Teubner, Stuttgart 1974) p. 1042
25.51 R. A. Street, J. C. Knights, D. K. Biegelsen: Phys. Rev. B **18**, 1880 (1978)
25.52 D. J. Dunstan, F. Boulitrop: Phys. Rev. B **30**, 5945 (1984)
25.53 K. Morigaki: J. Non-Cryst. Solids **141**, 166 (1992)
25.54 R. Stachowitz, M. Schubert, W. Fuhs: J. Non-Cryst. Solids **227–230**, 190 (1998)
25.55 C. Ogihara: J. Non-Cryst. Solids **227–230**, 517 (1998)
25.56 T. Aoki, T. Shimizu, S. Komedoori, S. Kobayashi, K. Shimakawa: J. Non-Cryst. Solids **338–340**, 456 (2004)
25.57 M. Yoshida, M. Yamaguchi, K. Morigaki: J. Non-Cryst. Solids **114**, 319 (1989)
25.58 M. Yoshida, K. Morigaki: J. Phys. Soc. Jpn. **58**, 3371 (1989)
25.59 B. A. Wilson, P. Hu, T. M. Jedju, J. P. Harbison: Phys. Rev. B **28**, 5901 (1983)
25.60 C. Ogihara, H. Takemura, H. Yoshida, K. Morigaki: J. Non-Cryst. Solids **266–269**, 574 (2000)
25.61 H. Takemura, C. Ogihara, K. Morigaki: J. Phys. Soc. Jpn. **71**, 625 (2002)
25.62 M. Yoshida, K. Morigaki: J. Non-Cryst. Solids **59 & 60**, 357 (1983)
25.63 G. Pfister, H. Scher: Adv. Phys. **27**, 747 (1978)
25.64 H. Scher, E. W. Montroll: Phys. Rev. B **12**, 2455 (1975)
25.65 I. Solomon: In: *Amorphous Semiconductors*, ed. by M. H. Brodsky (Springer, Berlin Heidelberg New York 1979) p. 189
25.66 K. Lips, C. Lerner, W. Fuhs: J. Non-Cryst. Solids **198–200**, 267 (1996)
25.67 M. Stutzmann, M. S. Brandt, M. W. Bayerl: J. Non-Cryst. Solids **266–269**, 1 (2000)
25.68 S. R. Elliott: In: *Material Science and Technology*, Vol. 9, ed. by R. W. Cahn et al. (VCH, Weinheim 1991) p. 376
25.69 A. Feltz: *Amorphous Inorganic Materials and Glasses* (VCH, Weinheim 1993)
25.70 H. Hosono, H. Maeda, Y. Kameshima, H. Kawazoe: J. Non-Cryst. Solids **227–230**, 804 (1998)
25.71 R. A. Street: Adv. Phys. **25**, 397 (1976)

25.72 B. C. Cavenett: J. Non-Cryst. Solids **59 & 60**, 125 (1983)
25.73 J. Ristein, P. C. Taylor, W. D. Ohlsen, G. Weiser: Phys. Rev. B **42**, 11845 (1990)
25.74 D. Mao, W. D. Ohlsen, P. C. Taylor: Phys. Rev. B **48**, 4428 (1993)
25.75 N. Kishimoto, K. Morigaki: J. Phys. Soc. Jpn. **46**, 846 (1979)
25.76 P. G. LeComber, D. I. Jones, W. E. Spear: Philos. Mag. **35**, 1173 (1977)
25.77 H. Overhof, W. Beyer: Philos. Mag. B **44**, 317 (1983)
25.78 D. I. Jones, W. E. Spear, P. G. LeComber: J. Non-Cryst. Solids **20**, 259 (1976)
25.79 N. F. Mott: J. Phys. C **13**, 5433 (1980)
25.80 W. E. Spear, P. G. LeComber: Philos. Mag. **33**, 935 (1976)
25.81 W. Beyer, J. Stuke: In: *Proc. Int. Conf. on Amorphous and Liquid Semiconductors, 1973*, ed. by J. Stuke (Taylor & Francis, London 1974) p. 251
25.82 L. Friedman: J. Non-Cryst. Solids **6**, 329 (1971)
25.83 D. Emin: Philos. Mag. **35**, 1189 (1977)
25.84 N. Tohge, T. Minami, Y. Yamamoto, M. Tanaka: J. Appl. Phys. **51**, 1048 (1980)
25.85 L. Tichy, H. Ticha, A. Triska, P. Nagels: Solid State Commun. **53**, 399 (1985)
25.86 K. Shimakawa, A. Kolobov, S. R. Elliott: Adv. Phys. **44**, 475 (1995)
25.87 K. Kimura, K. Murayama, T. Ninomiya: J. Non-Cryst. Solids **77, 78**, 1203 (1985)
25.88 D. L. Staebler, C. R. Wronski: Appl. Phys. Lett. **31**, 292 (1977)
25.89 I. Hirabayashi, K. Morigaki, S. Nitta: Jpn. J. Appl. Phys. **19**, L357 (1980)
25.90 H. Dersch, J. Stuke, J. Beichler: Appl. Phys. Lett. **38**, 456 (1981)
25.91 M. Stutzmann, W. B. Jackson, C. C. Tsai: Phys. Rev. B **32**, 23 (1985)
25.92 C. Godet, P. Roca i Cabarrocas: J. Appl. Phys. **80**, 97 (1996)
25.93 H. M. Branz: Phys. Rev. B **59**, 5498 (1999)
25.94 K. Morigaki, H. Hikita: Solid State Commun. **114**, 69 (2000)
25.95 K. Morigaki, H. Hikita: J. Non-Cryst. Solids **266–269**, 410 (2000)
25.96 K. Morigaki, H. Hikita: *Proc. Int. Conf. on Physics of Semiconductors*, ed. by T. Ando N. Miura (Springer, Berlin Heidelberg New York 2000) p. 1485
25.97 C. Ogihara, H. Takemura, T. Yoshimura, K. Morigaki: J. Non-Cryst. Solids **299–302**, 637 (2002)
25.98 K. Morigaki, H. Hikita, H. Takemura, T. Yoshimura, C. Ogihara: Philos. Mag. Lett. **83**, 341 (2003)
25.99 K. Morigaki, H. Hikita: J. Non-Cryst. Solids **299–302**, 455 (2002)
25.100 T. Gotoh, S. Nonomura, M. Nishio, S. Nitta, M. Kondo, A. Matsuda: Appl. Phys. Lett. **72**, 2978 (1998)
25.101 Y. Zhao, D. Zhang, G. Kong, G. Pan, X. Liao: Phys. Rev. Lett. **74**, 558 (1995)
25.102 H. Fritzsche: Solid State Commun. **94**, 953 (1995)
25.103 R. Biswas, Y. P. Li: Phys. Rev. Lett. **82**, 2512 (1999)
25.104 K. Morigaki: Res. Bull. Hiroshima Inst. Tech. **35**, 47 (2001)
25.105 M. Yamaguchi, K. Morigaki: Phys. Rev. B **55**, 2368 (1997)
25.106 C. Ogihara, H. Ohta, M. Yamaguchi, K. Morigaki: Philos. Mag. B **62**, 261 (1990)
25.107 M. Yamaguchi, C. Ogihara, K. Morigaki: Mat. Sci. Eng. B **97**, 135 (2003)
25.108 A. C. Gossard, M. Sundaram, P. F. Hopkins: In: *Semiconductors and Semimetals*, Vol. 40, ed. by A. C. Gossard (Academic, Boston; Tokio 1994) Chap. 2
25.109 N.-M. Park, C.-J. Choi, T.-Y. Seong, S.-J. Park: Phys. Rev. Lett. **86**, 1355 (2001)
25.110 J. Koga, K. Nishio, T. Yamaguchi, F. Yonezawa: J. Phys. Soc. Jpn. **70**, 3143 (2001)
25.111 R. Ionov, D. Nesheva, D. Arsova: J. Non-Cryst. Solids **137&138**, 1151 (1991)
25.112 R. Ionov: Ph. D. Thesis. Ph.D. Thesis (Technical Univ., Sofia 1993)
25.113 H. Hamanaka, S. Konagai, K. Murayama, M. Yamaguchi, K. Morigaki: J. Non-Cryst. Solids **198–200**, 808 (1996)